

# Tensile Response of Hoop Reinforced Multiaxially Braided Thin Wall Composite Tubes

Sree Shankhachur Roy<sup>1,2</sup> · Prasad Potluri<sup>1,2</sup> ·  
Constantinos Soutis<sup>2,3</sup>

Received: 3 October 2016 / Accepted: 2 November 2016 / Published online: 20 December 2016  
© The Author(s) 2016. This article is published with open access at Springerlink.com

**Abstract** This paper presents the tensile response of thin-walled composite tubes with multi-axial fibre architecture. A hybrid braid-wound layup has the potential to optimise the composite tube properties, however, stacking sequence plays a role in the failure mechanism. A braid-winding method has been used to produce stacked overwound braid layup  $[(\pm 45^\circ/0^\circ)_5/90^\circ_4]_T$ . Influence of stacking sequence on premature failure of hoop layers has been reported. Under tensile loading, a cross-ply composite tube with the alternate stacking of hoop and axial fibre show hoop plies splitting similar to the overwound braided composite tube. However, splitting has been restricted by the surrounding axial plies and contained between the adjacent axial fibre tows. This observation suggests hoop layers sandwiched between braid layers will improve structural integrity. A near net shape architecture with three fibre orientation in a triaxial braid will provide additional support to prevent extensive damage for plies loaded in off-axis. Several notable observations for relatively open braid structures such as tow scissoring, high Poisson's ratio and influence of axial tow crimp on the strain to failure have been reported. Digital Image Correlation (DIC) in conjunction with surface strain gauging has been employed to capture the strain pattern.

**Keywords** Braid · Filament winding · Braid-winding · Hoop · Axial · Triaxial · Composite · Tube · Tensile · DIC · Surface strain · Crimp · Stacking

---

✉ Sree Shankhachur Roy  
shankhachur.roy@manchester.ac.uk

<sup>1</sup> Robotics and Textile Composites Group, School of Materials, University of Manchester, Manchester, UK

<sup>2</sup> Northwest Composites Centre, University of Manchester, Manchester, UK

<sup>3</sup> Aerospace Research Institute, University of Manchester, Manchester, UK

## 1 Introduction

Cylindrical composite structures such as pressure vessels, tubes, pipes, shafts etc. are widely manufactured using filament winding technology. It is an established method of fabrication in the industry compared to other techniques such as fabric or tape wrapping and braiding for developing composite tubes. Filament winding (FW) is a popular choice because of its manufacturing feasibility and simplicity. Composite tube is often fabricated based on stiffness and strength requirement, in many cases with the requirement of multiaxial reinforcement architecture. Conventional FW process is able to manufacture preforms with fibres at  $\pm\alpha$  and hoop (near  $90^\circ$ ) direction (Fig. 1c). However, the process has a limitation in placing axial fibres (at  $0^\circ$ ) along the longitudinal axis of the tube. In contrast, braiding [1] has the capability of introducing axial fibres in the preform structure. In addition, braiding process produces a structure with bidirectional helically interlaced fibres. The helix angle with respect to the tube axis which is also known as braid angle, can theoretically range between  $1^\circ$  and  $89^\circ$  [2]. Though the practical use of braid angle usually ranges between  $\pm 20^\circ$  to  $\pm 80^\circ$ , with  $\pm 80^\circ$  generating higher fibre crimp. Higher crimp is undesirable for composite structures when the in-plane properties are a priority. Eventually fibre undulations affects the composite structural strength [3–5]. Whereas FW layups have little or almost no undulation and can conveniently produce hoop reinforcement. Therefore employing braiding technique for near hoop fibre placement or using FW for axial fibre deposition is not desirable. The respective limitations of both braiding and FW create the possibility for fabricating preforms by combining both layup techniques to optimise the fibre angles required to fabricate preforms for a tubular composite.

In this research thin-wall, composite tubes with carbon fibre reinforced epoxy were developed. In order to understand the fundamental material properties, the tubes were subjected to uniaxial tensile loading. Fibre preforms were developed using both braiding and FW techniques. A multiaxial layup with configuration  $[(\pm 45^\circ/0^\circ)_5/90^\circ_4]_T$  was produced using braid-winding and a triaxial quasi-isotropic layup  $[(\pm 60^\circ/0^\circ)_7]_T$  was produced using triaxial

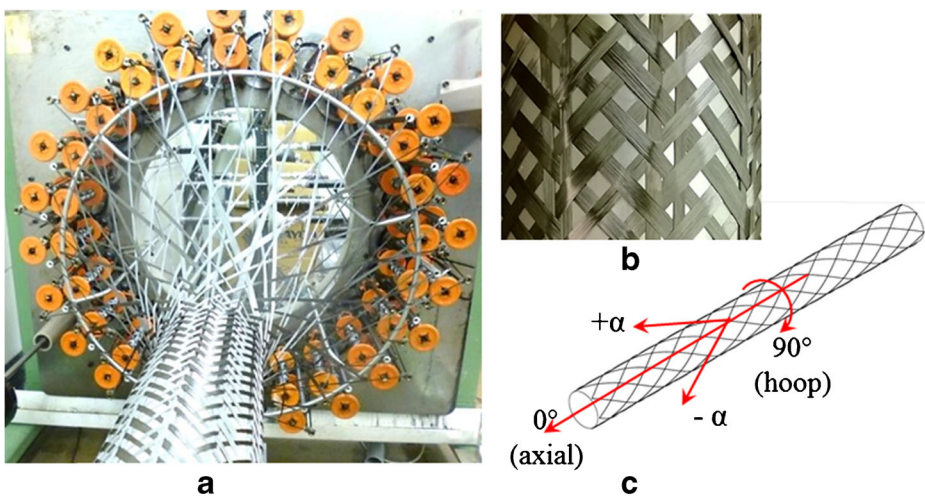


**Fig. 1** (a) Maypole braiding on a cylindrical core (b) Regular (2/2) braid structure (c) Schematic of fibre orientation for a cylindrical preform,  $\pm\alpha$  refers to braid angle in a preform with  $\pm\alpha/0^\circ$  triaxial braid architecture; fibres at  $\sim 90^\circ$  (hoop orientation) can be placed from filament winding

braiding. In the initial attempt, only two specimens of these two configurations were tested. Followed by the observations made from multi-axial specimen's premature failure, a simpler cross-ply layup was produced. In the cross ply layup, the hoop layers were placed in between the axial layers  $(0^\circ/90^\circ/0^\circ/90^\circ/0^\circ)_T$  with layup symmetry. The fabrication procedure of a cross-ply tubular preform shows the possibility of laying  $0^\circ$  fibres with a FW layup. In addition, a triaxially braided layup with fibre orientation  $[(\pm 45^\circ/0^\circ)_3]_T$ , similar to the one used for a multiaxis layup was produced for the study. A limited number of tests was carried out on these two types of composite tubes with triaxially braided and cross-ply layup. Failure process of hoop layup for two types of tubes was described with strain measurements from strain gauges as well as digital image correlation (DIC). Optical microscopy was carried out to observe and quantify fibre crimp within the specimen as the effect of crimp on mechanical properties was discussed. The measurements from DIC were correlated with the strain gauge data. Also, the failure process of the composite tubes was discussed using surface strain analysis.

## 2 Review of Braided Composites Under Tension

The literature on tensile response of braided tubes is limited and hence tensile response of flat braided laminates has also been included in the review. The reviews on braided composites cover tensile failure mechanism, the effect of fibre tow crimp, comparative studies with mechanical properties and local strain analysis.

The uniaxial tensile behaviour of glass fibre braided composite tube was studied using a biaxially braided layup with various helix angles [6]. Fibre tows in the composite with over  $\pm 45^\circ$  orientation show the scissoring effect as the matrix disintegrates when loaded in tension. This led to the formation of 'neck' and its propagation with a change in tube diameter.

A comparative analysis of triaxial braid (TB) composite with laminated composites showed lower strength in the direction of axial fibres when loaded biaxially [4]. Strength loss was suggested to be caused by the undulation of the helical fibres. The lower failure strain was explained in a follow-up study on the micromechanics of braided composite [7]. The study observed strain variation at different positions due to change in compliance with resin rich areas in the spacing between the fibre tows. This led to the average failure strain being low as well as influenced the ultimate strength as explained by the authors [7]. Since the current investigation has a similar open braided composite structure, the observation from this study was taken into consideration in order to prevent large resin rich areas during manufacturing.

Falzon and Herszberg [5] compared mechanical properties of TB composite with unidirectional (UD) laminate. Reduction of up to 30% tensile strength and 10% tensile modulus was reported for TB composite when compared with similar layup produced with UD tape. The axial fibre damage accounts for 20% loss in fibre strength as axial fibre tow was pulled out from preform and tested. Poisson's ratio was reported to be as high as 0.7 for  $\pm 45/0^\circ$  braid. With increasing braid angle decreasing Poisson's ratio was observed which was due to the increasing stiffness in the transverse direction. However, transverse deformation is also related to the longitudinal extension. As the composite structure had axial reinforcement, significant transverse deformation with necking as observed for a biaxial structure is not observed for TB composite [6]. The study does not provide any details on the relation between transverse and axial deformation. In addition, no effect of undulation on Poisson's ratio was observed when compared with UD as the ratio was similar.

Digital Image Correlation (DIC) method was used in two studies [8, 9] to analyse local strain variations for triaxially braided composite coupons. TB composite laminate was compared with that of a UD composite to analyse the failure process of the braided composite at meso level [8]. By using acoustic emission, the study showed that damage initiation is in correlation with that of UD composite when loaded in the direction of the axial fibre. For braided composite, crack appearance was observed in the surface layers indicating variation in stress-strain distribution from outer to inner layers. In addition, crack propagation was limited between the adjacent braided tow interlacements instead of running across the width. When loaded in the direction of axial fibre tows, the TB composite stress-strain response was observed [5, 8] to be linear and nonlinear response was observed for loading in other directions.

Microscopy images [10, 11] of TB composite laminate cross-section shows almost no crimp or waviness of the axial fibre for a multilayer stacked preform. However, for the open braided structures with less fibre coverage, the axial tow waviness need to be considered. West and Adams [12] studied triaxially braided composite under compression loading and observed 30% reduction in compressive strength due to the axial tow crimp. Rawal et al. [13] proposed a model considering the axial fibre tow crimp that can be calculated relating with the overall strain of the braid. The proposed equations were valid for braided structures at preform stage. The authors explained that axial tow crimp under tensile loading will not be straightened completely as the tows will experience radial stresses at the crossover points of the braided tows.

The review above is focused in relation to the observations and findings of this article. Relevant references were used during experimental work and analysis of results.

### 3 Experimental: Fabrication of Composite Tubes

#### 3.1 Braiding

Two-dimensional maypole braiding was used for developing tubular sleeves. A braided sleeve for reinforcement in composites can have three orientations within a single interlaced structure. Axial ( $0^\circ$ ) otherwise known as ‘inlay’ fibre tows lie in between the interlacement of diagonally oriented ( $\pm\alpha$ ) fibres. For composite tubes under tensile loading axial reinforcement along the tube axis is desired. Hence all the samples produced in this study had axial fibres in the preform. Two different configurations of braiding were carried out for the study was  $\pm 45^\circ/0^\circ$  and  $\pm 60^\circ/0^\circ$ . The approximate fibre weight for  $(\pm 60^\circ/0^\circ)_7$  braided preform was  $\sim 40\%$  and  $\sim 20\%$  in each bias and axial direction respectively. Later a  $(\pm 45^\circ/0^\circ)_3$  braided preform was developed with  $\sim 37\%$  fibres in each bias and  $\sim 26\%$  in the axial direction. The braid unit cell was large with uncovered surfaces with a cover factor of  $\sim 0.87$ . Hence layer positions in a stack were changed (Fig. 2). This improved axial fibre tows distribution around the circumference as well as the surface coverage.

A maypole braiding machine equipped with 48 bobbins was used to braid the preforms. By using an additional creel 24 axial yarns were supplied to produce a triaxial architecture. The preforming was carried out by using the T700 12k carbon fibre tows with  $7\mu\text{m}$  individual filament diameter. This carbon fibre has a tensile strength of 4900 MPa, modulus of 230 GPa and strain to failure of 2.1%. All braid structures had a regular 2X2 interlacement (Fig. 1b). A metal tube with  $\sim 100$  mm

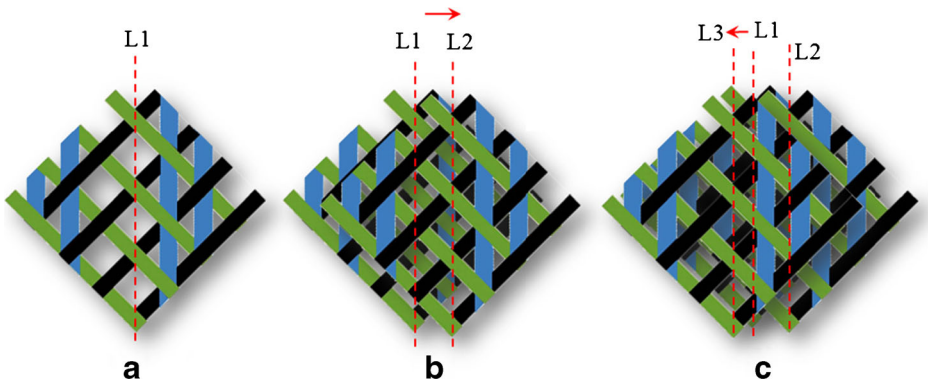


**Fig. 2** Schematic of a triaxial braid unit cell with change in layer positions in a stack (a) First layer with position indicated by dotted line (b) second layer shifted to distribute the axial fibre tows in between the tow spacing of the first layer (c) third layer shifted similarly with respect to the first layer

diameter was used as a core for multiple layers over braiding. The preform was left onto the metal tool during resin infusion and curing.

### 3.2 Over Winding of Braid (OWB)

In order to produce a layup with braid-winding, a triaxial braid with hoop winding is a suitable combination for developing composite tubes. Since the winding process stays separate from braiding, the layers of braid and filament winding were placed in two stacks eventually creating over winding on a braid layup. Four filament wound layers were placed on top of the braided layers producing a structure of  $[(\pm 45^\circ/0^\circ)_5/90^\circ_4]_T$ . A braid stack thickness of 1.95 mm was constructed by laying up five layers of braid onto the mandrel for OWB layup. The FW was carried out for this research in a winding equipment separate from a braiding machine but with a similar concept of a circumferential wrapping. Hoop winding ( $\sim 85^\circ$ ) was carried out on the braided  $(\pm 45^\circ/0^\circ)_5$  preform using this equipment.

### 3.3 Developing $0^\circ/90^\circ$ Cross-Ply (CP) Layup for Composite Tube

The overwound braid (OWB) composite tube had a stack of FW layers on top of the braid. Based on the observations on hoop layer splitting during tensile testing (discussed in Section 5), a different structure with hoop layers was produced. In this structure, hoop wound fibres were laid in between multiple layers of axial ( $0^\circ$ ) fibres to produce a cross-ply ( $0^\circ/90^\circ/0^\circ/90^\circ/0^\circ$ ) layup. Instead of combining with triaxial braid, only axial fibres were placed with hoop winding to observe the effect of single ply fibre on hoop layers when the composite is loaded in tension.

Placing  $0^\circ$  fibres with filament winding requires a special setup. In this process, the fibre tows were placed from one end of the mandrel to the other with the help of pins. It was carried out manually where the tows were guided using a nozzle. 24 pins have been placed around the circumference on each end in order to replicate the number of axial tows inserted in a single layer of triaxial braid. The wheel was mounted at the clamping end of the mandrel. As the tows were anchored around the pins on this wheel during the winding process it is termed as ‘anchor wheel’ (Fig. 3d). A compensating disc was placed at the end of the mandrel that kept the fibres in tension.

During the hoop winding, because of the diameter variation of the anchor wheel and mandrel, necessary axial fibre compensation as provided by the compensating disc (Fig. 3b and c).

For the CP layup, three layers of 24 axial tows were placed which is equivalent to that of a triaxially braided tube (TB). Although braiding was not carried out for this layup, the two layers of hoop winding were placed in between two layers of axial tows in order to understand the difference in failure process under tensile loading in comparison with the over wound braid type. The observations will also allow a possible braid-winding layup with three layers of triaxial braid replacing the layers of axial tows in CP configuration for future study.

### 3.4 Resin Infusion and Curing

The preform was impregnated with epoxy resin Araldite LY564 with hardener XB3486. The resin to hardener mixing ratio was 100 to 34. A vacuum assisted liquid resin infusion method (Fig. 4a) was used for wetting the preform on the tubular mandrels. The resin-infused preform was then cured at 80°C for 8 hours. Followed by curing and de-moulding, the composite tube was cut to the 140 mm length for testing preparation.

### 3.5 Braided Preform and Composite Material Characterization

A multi-layer braided preform stack thickness build up with respect to a single layer thickness is not directly proportional. The change in total braid stack thickness can be quantified using nesting factor [14, 15]. Thickness reduction of  $(\pm 45^\circ/0^\circ)_5$  braided layup due to nesting was ~21% with a final stack thickness of ~1.95 mm. In addition, during preforming of OWB layup

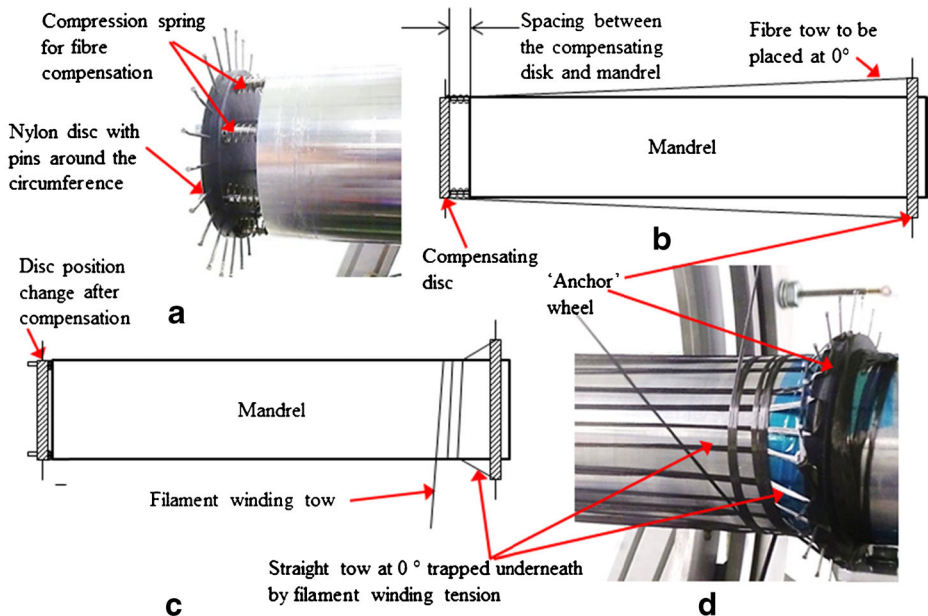


**Fig. 3** (a) Compensating disc at the end of the tubular mandrel to provide fibre tow tension and compensation (b) Schematic of a mandrel with straight fibres placed between the anchor wheel and compensating disc before winding (c) Schematic of compensation process after winding is started (d) Winding on the mandrel after the axial fibre tows (0°) were placed at ~13 mm spacing.

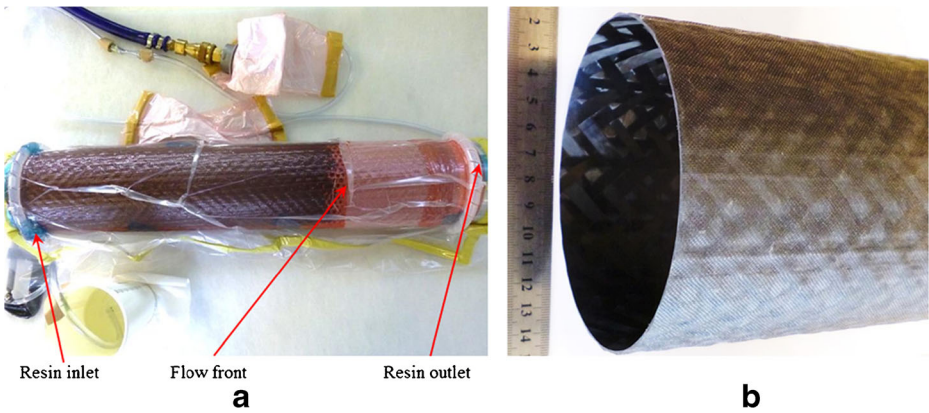


**Fig. 4** (a) Resin infusion setup (b) An image of a triaxially braided composite tube

the fibre tension consolidates the braid structure and the braid stack thickness reduces further. The final dry preform thickness was 2.27 mm with four layers of winding. Preform thickness reduction due to nesting for the  $(\pm 60^\circ/0^\circ)_7$  and  $(\pm 45^\circ/0^\circ)_3$  was about 18% and 19% respectively. Despite layer nesting, large resin rich area was observed from microscopy image within braided stack of OWB structure due to lack of surface coverage (Fig. 5).

Composite tube wall thickness was measured at 16 different points and average values were used for calculation. Specimens were analysed using matrix digestion method for fibre volume fraction (FVF) according to the standard ASTM D3171 [16]. The fibre and void volume fraction for the composite tubes are presented in Table 1. Specimen dimension for the fibre volume fraction analysis was minimum 20 mm × 20 mm. As the  $(\pm 45^\circ/0^\circ)_3$  preform did not have full surface coverage, the FVF was comparatively less ( $58\% \pm 1.8$ ) than other constructions. In addition, as the braid structure was open and the positions of the layers in a stack were changed to distribute the fibre tows around the surface, local FVF will be non-homogeneous. This can be observed from the Fig. 6a microscopy image that shows significant thickness variation around the specimen. Resin rich areas can be observed on the wall which will

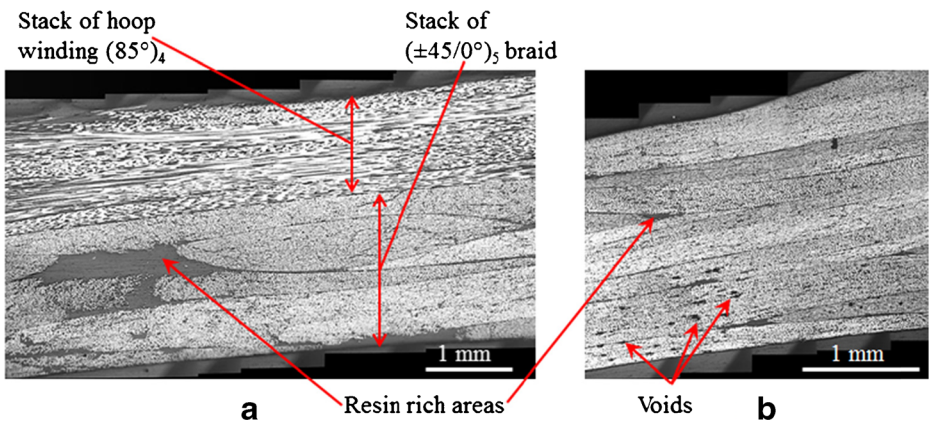


**Fig. 5** Tube wall cross section images of (a) Over wound braid (OWB) layout  $[(\pm 45^\circ/0^\circ)_5/90^\circ_4]_T$  (b) Triaxially braided quasi-isotropic (TQI) layout  $[(\pm 60^\circ/0^\circ)_7]_T$

**Table 1** Preform and composite tube geometry (average values)

Sample type and notation	Overwound braid (OWB)	Triaxial quasi-isotropic braid (TQI)	Triaxial braid (TB)	Cross ply (CP)
Preform Layup orientation	$(\pm 45^\circ/0^\circ)_3/90^\circ_4$	$(\pm 60^\circ/0^\circ)_7$	$(\pm 45^\circ/0^\circ)_3$	$0^\circ/90^\circ/0^\circ/90^\circ/0^\circ$
Preform thickness (mm)	2.27	3.10	1.18	0.78
Composite tube wall thickness (mm)	$1.84 \pm 0.3$	$2.10 \pm 0.3$	$0.71 \pm 0.11$	$0.49 \pm 0.06$
Thickness reduction (%)	19	32	40	37
Density ( $\text{g}/\text{cm}^3$ )	1.53	1.51	1.51	1.53
Total FVF (%)	61.70	61.40	58.00	60.50
FVF at $\alpha^\circ$ orientation (%)	16.35	24.56	21.40	-
FVF at $0^\circ$ orientation (%)	11.54	12.28	15.14	26.80
FVF at $90^\circ$ orientation (%)	17.40	-	-	33.70
VVF (%)	1.0	2.1	1.5	1.3

decrease the local FVF. The cross section image also shows consolidated thicker wall section with higher local FVF. Void volume fractions (VVF) for all types of tubes were less than 2%.

Optical microscopy was carried out to observe the cross section of composite tube walls. Significant wall thickness variation around the tube circumference can be observed from  $(\pm 45^\circ/0^\circ)_3$  specimen cross section image (Fig. 6a). Part of the wall had resin rich zones between layers (Fig. 6b) as well as nested and consolidated sections (Fig. 6c). The TQI  $(\pm 60^\circ/0^\circ)_7$  composite wall cross-section image shows the presence of microvoids (Fig. 5b) at the bottom layers. On the other hand, large resin rich area between the braided layers can be observed for over wound braid structure (Fig. 5a).

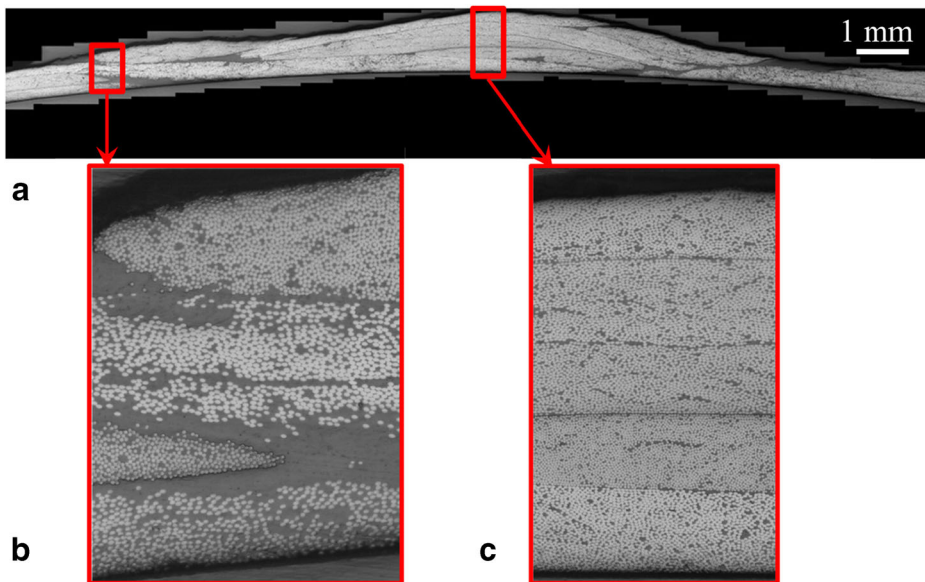


**Fig. 6** Optical microscopy images of a  $(\pm 45^\circ/0^\circ)_3$  composite tube wall cross section showing (a) Varying wall thickness (b) resin rich areas between layers are observed (c) consolidated layers



## 4 Tensile Testing and Results

### 4.1 Tensile Testing of Composite Tubes

The composite tube test specimen gauge length was  $101 \pm 1$  mm. Each specimen was mounted on the ASTM recommended test jig (Fig. 7a), bonded at both ends with inner and outer fixture using a structural adhesive over a length of 20 mm. In order to measure strain, strain gauge rosettes were placed in the centre of the gauge length. Each rosette had three strain gauges placed at an orientation of  $0^\circ/45^\circ/90^\circ$ . Three rosettes were mounted on the tube outer circumference  $120^\circ$  apart from each other.

The composite tube specimens were tested following ASTM D5450 [17]. A hydraulically actuated 300 kN Instron 8802 testing equipment (Fig. 7b) was used for testing purpose. The tests were carried out at a constant crosshead displacement rate of 1.3 mm/min. Ultimate tensile strength (UTS) values were calculated from the maximum load and the cross-sectional of the tube specimen wall. The axial strains and circumferential strains were calculated separately from each strain gauge rosettes. The average principal strains were calculated by averaging the strain values from three rosettes.

### 4.2 Surface Strain Measurement During Testing

A photogrammetric method was used to obtain the full field deformation of the specimen surface during the test. Digital image correlation (DIC) equipment (Q-400 system developed by Dantec Dynamics) was used for surface strain measurement. The system uses two cameras to take images of the specimen surface. After a certain load interval, digital images were taken during the test. Evaluation of the images and data extraction, ISTRA 4D software was used. The software recognises the speckle pattern painted on the outer surface of the specimen. Before the test, reference images were taken by the cameras after the calibration of the system. During deformation of the specimen, the Q-400 system determines the position of the pattern,

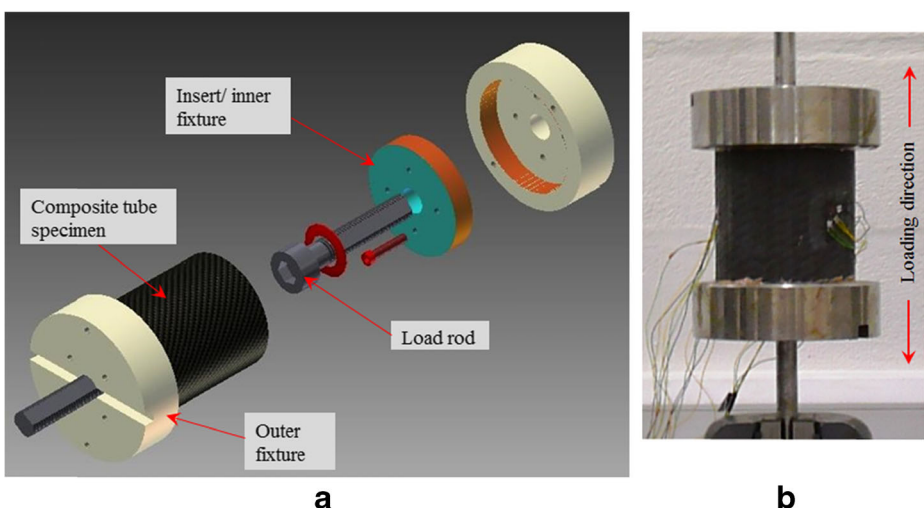


**Fig. 7** (a) CAD image of tube specimen with ASTM recommended fixture assembly (b) Composite tube specimen mounted on the tensile testing equipment

therefore, the pattern appearance with respect reference images. The displacement field between the reference and the deformed image is measured on a virtual grid defined in the reference image. Each grid points are in the centre of a small square area within the region of focus called facet. The software tracks and calculates surface strains in two methods. One of the methods involves three-dimensional distortions of facets and in the other method, the software calculates the gradient of the deformation. In this study, due to the flaws in speckle pattern, some parts of 3D image reconstruction were incomplete for the specimens. However, the data were extracted effectively from the fully constructed region and excluding the incomplete parts.

A reconstructed image would appear with strain maps in a different colour as shown in Fig. 8a. The red and yellow regions of the image are presenting the strain concentration (over  $0.02 \epsilon$ ) when loaded. These high-strain regions lie diagonally and parallel to each other replicating the pattern of  $\pm 45^\circ$  fibre layup. This phenomenon relates to a previous study [18] on triaxial braided flat composite in which authors observed localised high strain concentration from surface strain measurement. These high strain concentrated regions also act as the damage initiation point. The red regions are located at certain interval indicating the fibre crossover or interlacing points of the braid where the axial tows are located as well.

The surface area considered for evaluating the images recorded by DIC software was large enough for both the cases to cover more than one unit cell along the length and circumference. As the fibre reinforcement was located in a different direction, for TB tube there were areas of the tube with tow crossover points where two biaxial tows crossed each other keeping an axial tow in the middle. In addition, there were areas where only biaxial tows or a combination of biaxial and axial tows lay in different layers without any crossover. Although from the evaluated region average surface strain was measured, further investigation on a local variation on axial and transverse strain was carried out. The surface strain data was extracted at different stress levels along the length of a line drawn on to the DIC image of the specimen. The end to end distance of these lines was often stretched several adjacent unit cells of the braid structure on the specimen.

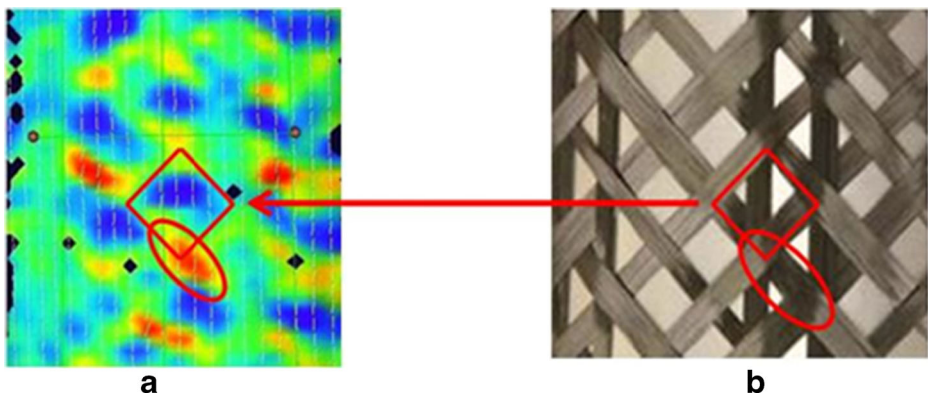


**Fig. 8** (not to scale) (a) Apparent replication of braid cells in the form of strain illustration created by DIC software on a composite tube (To observe the colour representation of surface strain for the analysis in the rest of the article, the reader is referred to the web version of the article) (b) A dry preform image to illustrate the fibre architecture

### 4.3 Test Results

Multiple specimens of CP and TB layup were tested under tensile loading. A summary of the material properties for all tube specimens tested is presented in Table 2.

## 5 Analysis of Test Results and Observation

### 5.1 Braided and Overwound Braided Composite Tube

A specimen of both TQI and OWB composite tube were tested under tensile loading. The ultimate strength of TQI and OWB tubes were 385.4 MPa and 355.4 MPa, respectively. As the FVF of the axial fibres in both the specimen were close (~11.5% for OWB and ~12.3% for TQI) no significant strength difference was observed. However, the tensile modulus of OWB tube was ~20% higher than that of TQI structure. One of the major factors that contributed to a comparatively higher modulus is the alignment of bias fibres ( $\pm 45^\circ$ ), the arrangement of those were closer to the axis of loading when compared to  $\pm 60^\circ$  plies of TQI layup.

The TQI specimen failed with delamination of all the braid layers in the wall. In addition, under tensile loading the braided fibres moved in the radial direction (Fig. 9b and c) which contributed to the failure process. Fibre tow failures with transverse cracks were observed at the interlacing point (Fig. 9b). In addition splitting of fibre tows across the width were observed for at  $\pm 45^\circ$  (Fig. 9c).

The stress-strain graph for TQI tube from the strain gauge and the surface strain values from DIC against stress points were plotted (Fig. 9a). Both of these graphs show a steady rise in strain with the stress but an exception was observed between 180 and 200 MPa for the surface strains. There was a sudden increase in strain at that range without any drop in load which is explained using surface strain evaluation at a different point on the specimen (Fig. 10a).

In Fig. 10a the graphs illustrate strains at five different stress values, three of which are equal or less than 50% of UTS (group 1) and two of those are over 75% of UTS (group 2). Each of these shows a peak region along with a base region which is correlated with the area in between two densely stacked crossover points and the fibre crossover points respectively. On the composite tube, in some places the wall thickness was as low as 1.7 mm in contrast with the crossover points which had a wall thickness up to 2.4 mm. The graphs show a significant increase in strain at higher stress especially in the area in between the crossover points due to stress concentration. However, on the crossover points, the graph for 190MPa shows high strain

**Table 2** Tensile properties of composite tubes

Specimen type	Number of specimens tested	Ultimate tensile stress, $\sigma_{ult}$ (MPa)	Tensile modulus of Elasticity, E (GPa)	Poisson's ratio, $\nu_{21}$	Average strain at failure (%)
CP (0°/90°/0°/90°/0°) <sub>T</sub>	5	670.7 ± 18.6	49.5 ± 7.1	0.11 ± 0.04	1.3 ± 0.2
TB [(±45°/0°) <sub>3</sub> ] <sub>T</sub>	3	635.4 ± 34.7	35.3 ± 2.2	0.77 ± 0.05	1.8 ± 0.2
OWB [(±45°/0°) <sub>3</sub> /90° <sub>4</sub> ] <sub>T</sub>	1	355.4	37.6	0.4	0.58*
TQI [(±60°/0°) <sub>7</sub> ] <sub>T</sub>	1	385.4	29.9	0.24	1.36

\*Electric strain gauge failed prematurely due to splitting of the 90° surface ply

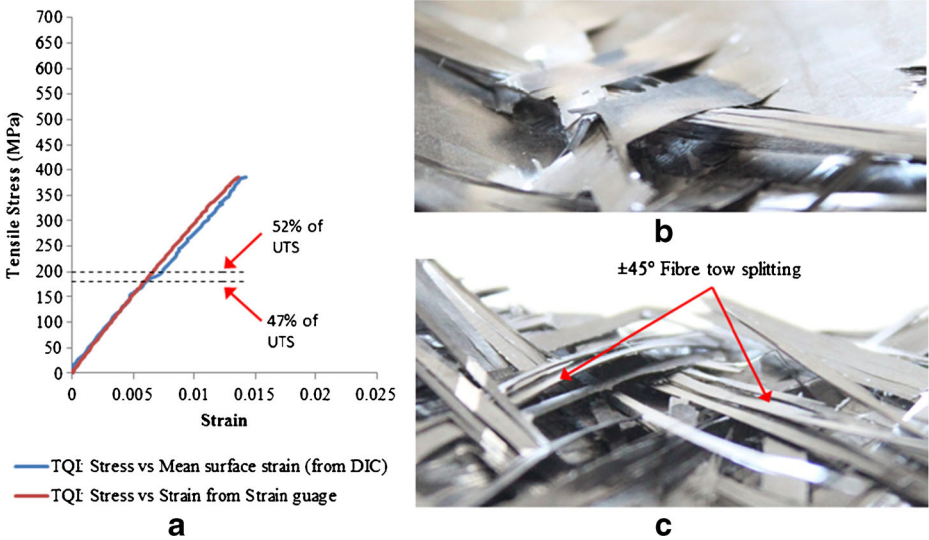


**Fig. 9** (a) For triaxially braided quasi-isotropic (TQI) tube, the surface strain values showing good correlation with strain gauge data up to 50% of UTS. The deviation in strain was observed between 180–200MPa (b) The tube after failure shows tendency of bias ( $\pm 45^\circ$ ) fibre moving out of the tube wall surface delaminating within and between braid layers (c) Bias fibre splitting across the tow width

with the increase in peak strains. It explains that the region which is a stack of fibre crossover points has gone through higher deformation for a very small change in stress. The legend (Fig. 10a) 17.5 and 16.9 (similarly 9.5 and 10.1) shows a shift in the peak of the graph at two

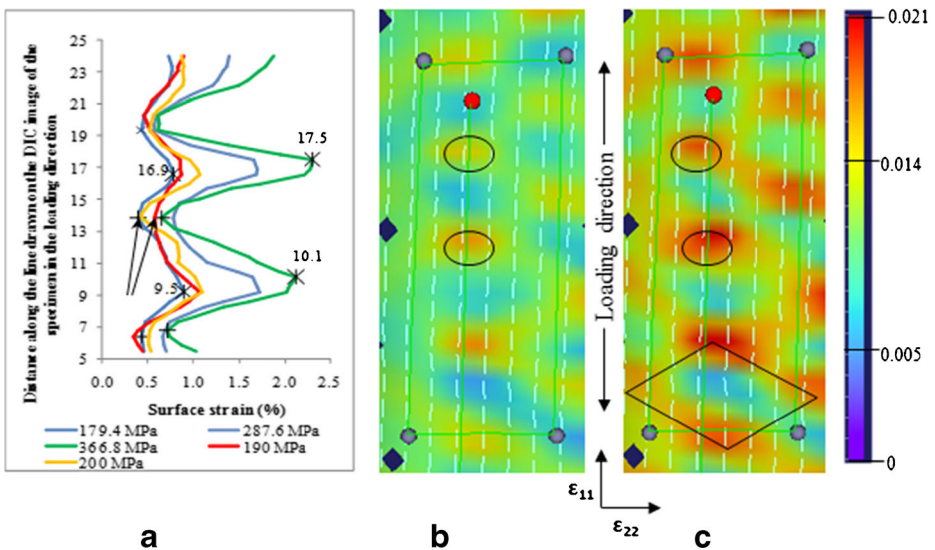


**Fig. 10** (a) Surface strain along a line at different stress values, arrows pointing to a shift in graph pattern at 190 MPa which correlated with the sudden increase in surface strain shown in Fig. 8a; Surface strains as high as 2% is observed whereas the average failure strain was only 1.4% (b) High strain state at parts of the specimen at about 366 MPa (~75% of UTS). The diamond shape in fig (c) in the form of a braid unit cell is illustrated by the strain concentrated regions. The oval shapes indicate high strain regions caused by gradual stress concentration between two crossover points.

different stress values indicating movement of a certain area on the specimen possibly caused by the straightening of any fibre waviness which is also known as crimp interchange [19].

From the graph in Fig. 10a, it also appears that during the test different areas of the specimen strained more than the average failure strain of 1.4% without any major damage. The similar chart also shows that for 179.4 MPa and 366 MPa the position of peak and base points moved along the line which indicates possible crimp interchange after the matrix cracking had occurred.

As the hybrid layup of OWB tube was tested under tensile loading, the strain recording from strain gauge was interrupted in the middle of the test. The interruption was caused by the surface crack appearance. The strain gauge recorded the last strain point at 214.9 MPa which is about 60% of the UTS of OWB tube. Under the tensile loading, the filament wound layer stack had gone through different extension in comparison with the stack of the triaxial braid as the braid layers had fibre oriented in the direction of loading. In contrast, the load was acting in the transverse direction of the hoop wound fibres. The matrix cracks within the filament wound layers created by the accumulation of local damage led to the transverse cracks on the outer hoop layers. This observation was validated from the reconstructed DIC images at different stress (Fig. 12). The transverse failure is also a result of the volume effect at ply level as the four hoop layers were stacked all together. These cracks split the hoop layers which later appeared in form of ‘band spiral’ failure mode (11c). During this splitting event, the de-bonding between the split bands and the inner braid structure took place. The de-bonded FW layer lies completely separate from the disintegrated stack of braid layers which was observed from the optical image (Fig. 11b) of the tube wall. Also during the test, the load-extension graph showed the uninterrupted increase in load for OWB structure. This explains that as the FW layers split, the braid continued to take the load until failure. The fractured outer surface of the OWB specimen caused breakdown of strain gauges, therefore, it was not possible to obtain failure strain.

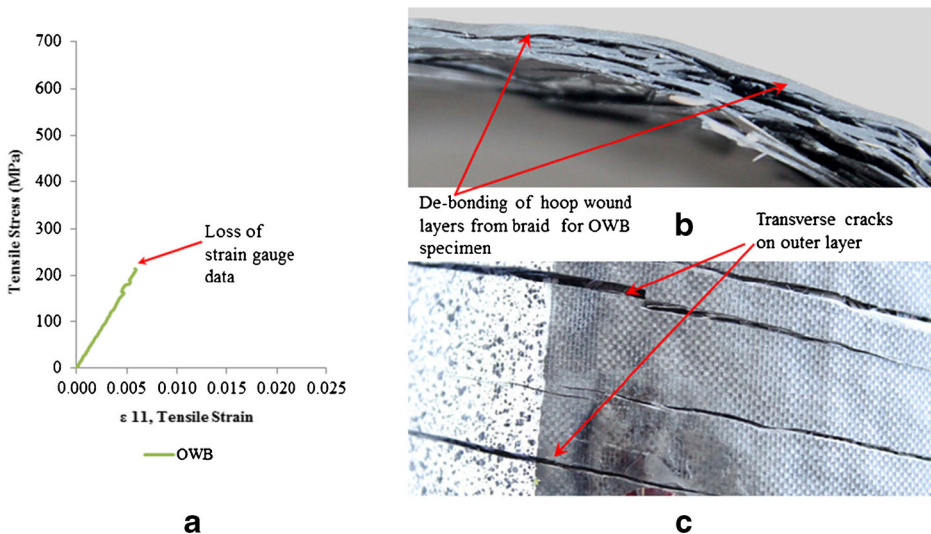


**Fig. 11** (a) Stress-strain for over wound braided (OWB) specimen, arrow indicates the point onwards strain gauge failed to record the deformation due to outer hoop layer splitting (b) OWB tube wall cross section after failure showing the hoop wound layers lying separately from the disintegrated braid (c) Appearance of transverse cracks on OWB specimen outer wall

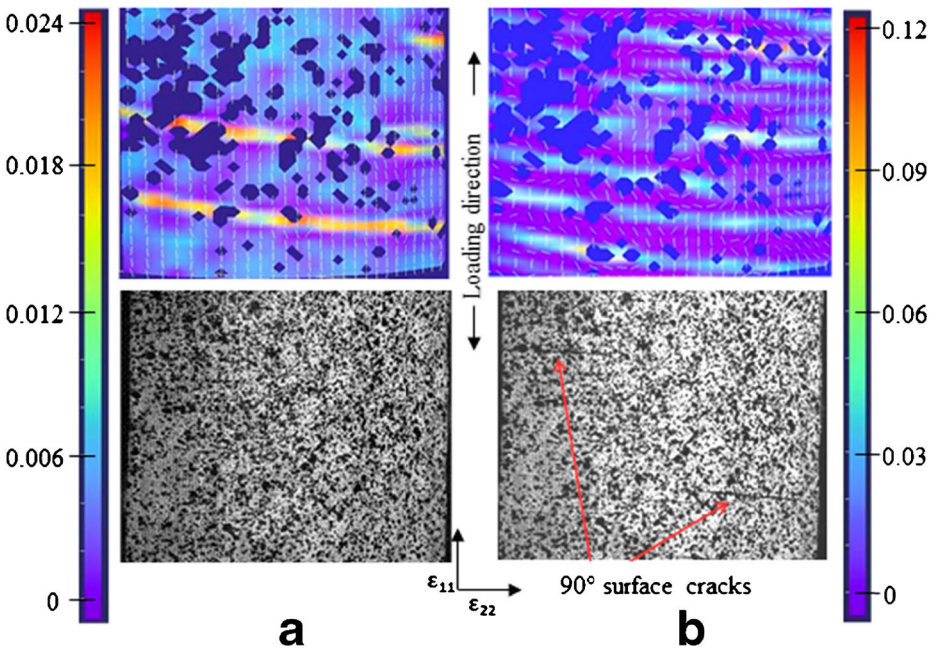


**Fig. 12** (a) At 60% of UTS, DIC reconstructed image with scale on the left and corresponding specimen image (b) At 90% of UTS, DIC image with scale on the right shows major strain concentrations in the pattern of hoop fibre around the circumference with rapid strain increase, the corresponding specimen image showing crack openings on the surface

### 5.2 TB ( $\pm 45^\circ/0^\circ$ )<sub>3</sub> Composite Tubes

The stress-strain graph for the triaxially braided composite tube is presented in Fig. 13a. High transverse deformation shows almost same axial and transverse strain. As a result, Poisson’s ratio calculated for this tube was highest (0.77) among all the specimens. The high transverse deformation

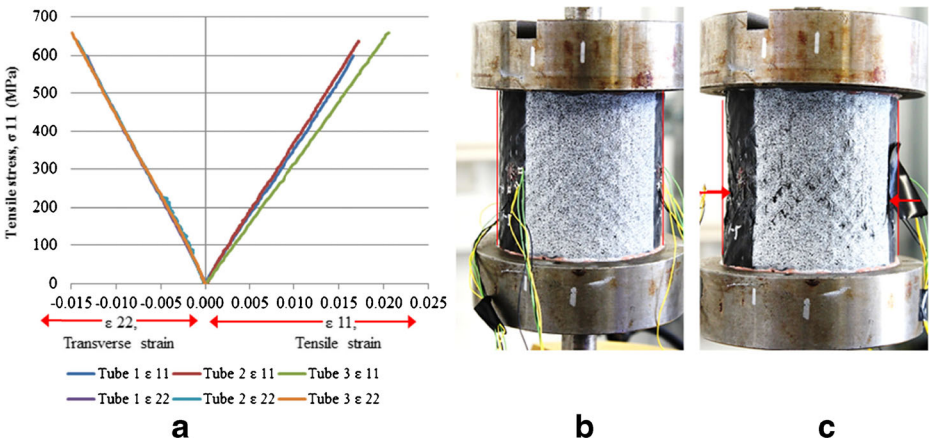


**Fig. 13** Tensile stress-strain (axial and transverse) graph for TB ( $\pm 45^\circ/0^\circ$ )<sub>3</sub> composite tubes (b) TB tube specimen before testing (c) after testing showing the diameter reduction at the centre indicating high transverse deformation of the tube structure

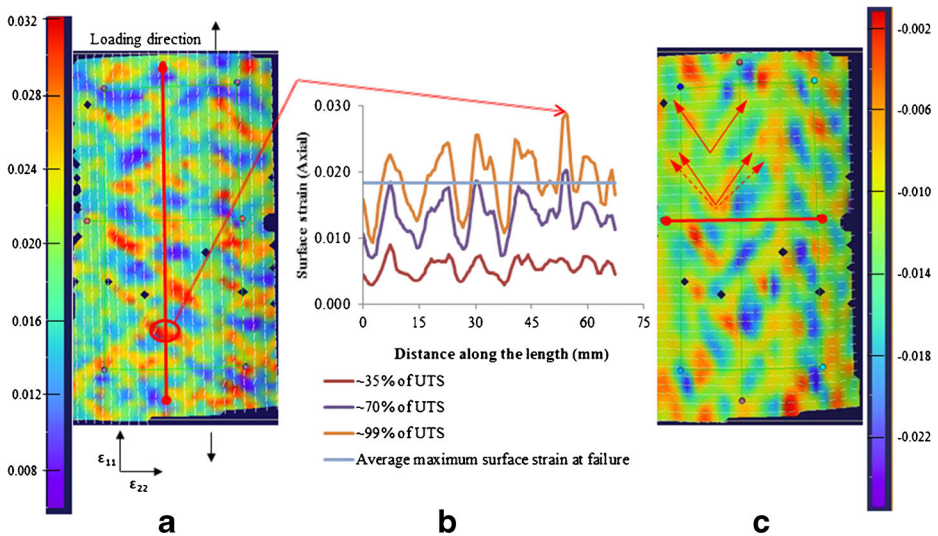


**Fig. 14** Surface strain analysis of TB ( $\pm 45^\circ/0^\circ$ )<sub>3</sub> composite tube (a) Axial strain map at 99% of UTS; strain was calculated along the red line in the middle of the image (b) at 3 different stress condition calculated strain along the length of the line shown in (a); graph for 99% of UTS indicating axial strain as high as 0.03 localized at the fibre crossover point (c) Transverse strain map image at 99% of UTS showing high contraction regions; Dotted arrow indicates initial fibre orientation about  $\pm 45^\circ$  from the strain map and solid arrows showing change in fibre orientation to about  $\pm 35^\circ$

was also observed from the DIC analysis as shown in Fig. 14c. Braided composite tube ‘necking’ is a phenomenon observed [6] for biaxially braided tube where the deformation of the tube forms ‘neck’ and the diameter narrows at the middle section. Although the TB tube had a triaxially braided reinforcement with axial fibres in the loading direction, the failed specimens did not retain the same diameter as the original one (Fig. 13b and c). Diameter necking was not as significant as a biaxial braided composite tube due to the presence of axial fibres. The axial tow crimp interchange under tensile loading allowed the specimen to have a significantly high tensile strain (average 2%, localised 3% measured from DIC). This tensile deformation led to helically interlaced bias ( $\pm 45^\circ$ ) fibres to shear. This eventually reduced the diameter in the middle of the tube which was evident from the fractured specimen (Fig. 13c).

### 5.2.1 Relation Between Axial tow Undulation and TB Composite Strain to Failure

In the case of a fully covered braid, usually the axial tow undulation and subsequent crimp for an axial tow is very low. In this study, the braid structure of a single layer was relatively open ( $\sim 87\%$  cover) with 15% axial FVF. During manufacturing, there was some axial fibre tow movement and also the distribution of these around the tube circumference was non-uniform. One of the microscopy images of the TB tube wall cross-section shows one axial tow (Fig. 15a and b). This image reveals that the tube wall has significant thickness variation and the axial tow crimp was as high as 0.7%. The thinner wall section during loading will experience higher stress concentration and subsequent higher strain during the test. Another cross-section image (Fig. 15c and d) from the same specimen shows two axial tows with less variation in thickness and axial tow crimp in the region of 0.15 to 0.2%.

Although some parts of the specimens had higher axial tow crimp, once the crimp interchange of axial tows with low undulation completes, these tows will start taking the load until the fibres in the

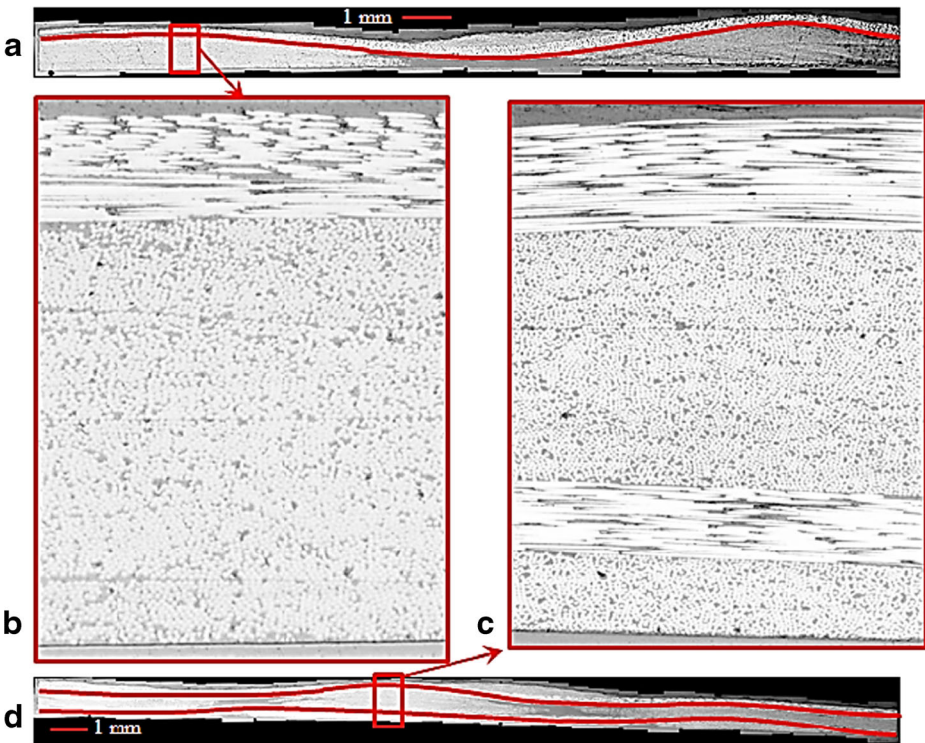


**Fig. 15** Optical microscopy images of TB ( $\pm 45^\circ/0^\circ$ )<sub>3</sub> composite tube wall cross section along the length of the tube i.e., along with the length of the axial tow (a) The line across the width indicating waviness of an axial tow with about 0.7% crimp (b) Close-up view of a section showing one layer of axial tow (c) Close-up view of another section from the same specimen with axial tows in two layers (d) Two lines indicating the locations and waviness of axial tows with about 0.15% and 0.2% crimp

composite reach the failure strain. Cross-ply layup will have lower undulation compared to an open braided structure. The failure strain for TB composite tubes is higher than that of the CP tube since the off-axis fibres contribute to the deformation by shearing. An additional contribution to higher failure strain comes from the higher crimp inherited in the axial tow of the TB tube; the average axial tow crimp was 0.35%. A crimp value of 0.35% will equate to an additional 0.0035 axial strain. This suggests that the TB specimen can support between 1.35% and 1.85% tensile strain before fracture, compared to 1.0–1.5% for the failure strain of the cross-ply specimen (Fig. 16). The measured strain to failure for the TB specimen ranged between 1.7% and 2.0%. This correlates well with the upper end (1.85%) estimated by accounting for axial tow crimp. The average surface strain at failure for one of the specimens was also calculated to be about 1.8% as shown in Fig. 14b. It should be noted that if the tube was loaded in axial compression then the tow crimp would be detrimental to its load carrying capability.

### 5.3 Observations on Cross-Ply Tube Structure

The FVF of the axial tow for CP and TB types of tubes were 27% and 15% respectively. Although the average ultimate strength of the CP tube was about 5% higher than that of TB, the tensile modulus was about 25% higher. The reason for lower modulus was a high transverse deformation of the TB type tube. Whereas despite having lower FVF of  $0^\circ$  fibres, the average strength was close to



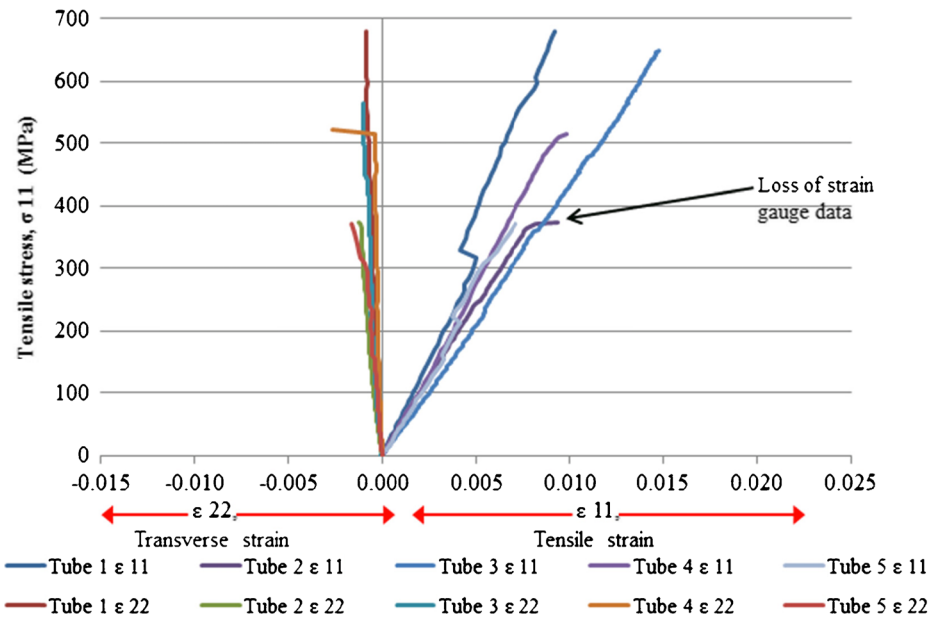


**Fig. 16** Tensile stress-strain (axial and transverse) graph for CP (0°/90°/0°/90°/0°) composite tubes

that of CP tube. As the TB tube deformed under loading, the  $\pm 45^\circ$  braided fibres changed orientation (to  $\pm 35^\circ$ ) towards the loading direction (Fig. 14c). This change in fibre orientation eventually contributed to the higher strength. In addition, Poisson’s ratio of CP tube was significantly lower than that of TB type tube as a result of very low transverse deformation.

Some of the graphs of CP tube (Fig. 16) do not show a continuously linear increase in average strain because of one or more sets of strain gauge failure as the specimens went through some degree

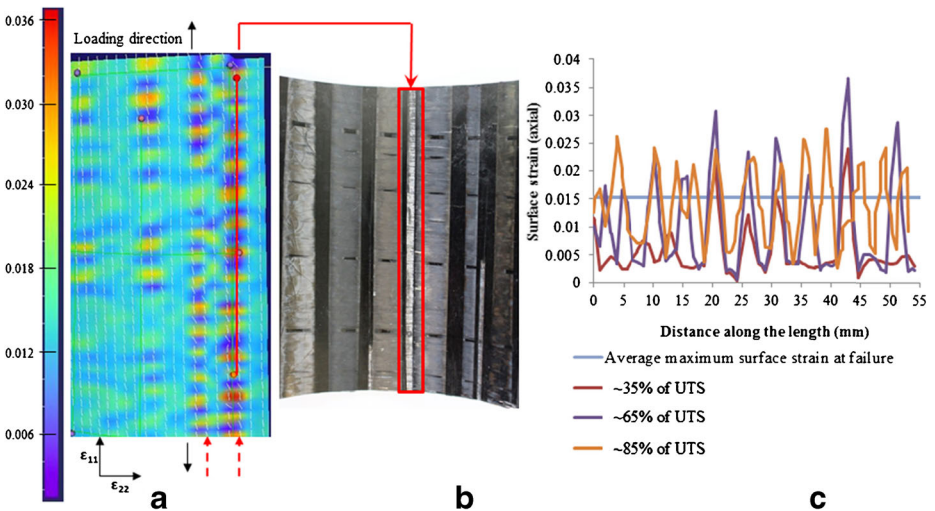


**Fig. 17** (a) Image at step before the specimen failure with high strain regions shown using dotted arrows (b) Axial fibre pull out from the inner wall of the CP tube after failure that lies opposite to the high strain region observed on the DIC strain map in (a); (c) At 3 different stress surface strain along the length of the line shown in (a); distance 0 mm indicates point on the line at top of the specimen

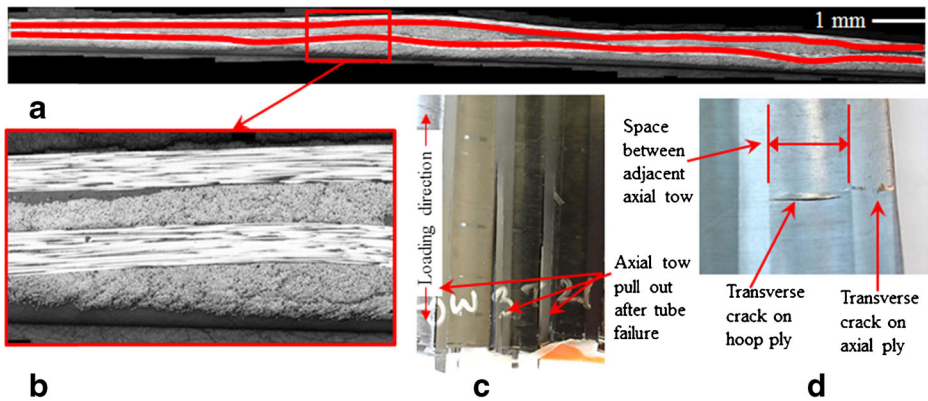


**Fig. 18** (a) Optical microscopy images of cross-ply composite tube wall cross section along the length of the tube. The lines across the width indicating waviness of an axial tow with about 0.1 to 0.3% crimp (b) A close-up view of the cross-section image (c) Axial tow pull out from inner wall of the tube after failure (d) Hoop ply transverse crack (~8.5 mm) located in between adjacent axial tows from another ply; transverse crack appearance on the axial tow on the side of the crack on hoop ply

of transverse failure. Hence ultimate strain at failure for CP tube in Table 2 was calculated after excluding two specimen data. Two of the CP specimens in the graph (Fig. 16) shows kink with strain drop which was caused due to the appearance of the transverse cracks which was later observed to be on the hoop layers.

The observation in one of the CP tube specimens after failure showed axial fibre pull out from the inner wall (Fig. 17b) that resembles the location with high strain as shown in Fig. 17a. Dotted arrows indicate axial tow position along which the high strain was clustered. Failed specimen of CP structure was inspected and transverse cracks were observed in the hoop wound layer. As the hoop layers were sandwiched between axial layers, the crack propagation was stopped by the axial tows. Axial tow spacing was about 13 mm (Fig. 3d) and the maximum transverse crack length on the hoop layer was observed about 8.5 mm. On the inner wall of the specimen at several positions, these cracks were observed. Some of the axial tows were failed with transverse splitting along the length and the locations of these were close to the transverse cracks of the hoop layers (Fig. 18d).

## 6 Concluding Remarks

Triaxially-braided, cross-ply and overwound braided composite tubes were used for this study under tensile loading. A braid structure with the uncovered surface was produced followed by a layer stacking that improved surface coverage and distribution of the axial tows around the circumference. An innovative method for placing axial fibre tows demonstrated the possibility of producing a cross-ply layup with hoop winding for cylindrical composite structures. Combining the process of hoop winding with braiding an overwound braid layup was produced. The braid wound layup was a two stacked preform and the failure process of this structure under tensile loading led to further investigation other layups.

Some interesting observations were noted from the mechanical tests conducted and the tube failure process under tensile loading. One of the major observations of this investigation was the early failure of hoop layers of a combined braid-filament wound layup. In order to understand the difference in failure process, a cross-ply layup composite tube was produced with hoop layers

sandwiched between the axial fibre layers. For the cross ply tube, hoop layer crack propagation was stopped by the surrounding axial tows. This observation suggests that a combined layup of triaxial braid and hoop winding with winding sandwiched in between the braid layers will provide improved structural integrity preventing transverse splitting like the one observed in the OWB structure. A similar over wound braid structure or a braided layup sandwiched between hoop layer stacks is likely to fail early.

For triaxially braided quasi-isotropic layup DIC was used for surface strain analysis. The average surface strain correlated with strain gauge values at the early stage of the test although variations were noted with surface strain map. Analysis of strain at different stress level was carried out to explain the change within the structure for the observed variation. DIC analysis for TB ( $\pm 45^\circ/0^\circ$ )<sub>3</sub> specimen showed biaxial fibre scissoring to change the braid angle to about  $\pm 35^\circ$ . This led to the higher tensile strength of TB specimens compared to CP tube although CP tube had the highest strength due to the higher axial fibre volume fraction. The relatively low fibre volume fraction of the axial layer in the TB tube led to the lower tensile modulus.

A large variation on local strains was observed for TB tube specimens that were due to the fibre tow spacing and open braid structure. From the previous studies by the authors, it was noted that for a fully covered triaxially braided composite, the axial tows show relatively low undulation and crimp. However, microscopy images for the open braid structure of TB specimens revealed that the axial tows had 0.1–0.7% crimp. The axial tow crimp interchange subjected to tensile loading allows the triaxial braid to fail at the higher axial strain. The TB specimens failed between 1.7% and 2%, the average of which was comparable to the upper range of predicted failure strain considering the axial tow crimp. The CP tube where the axial tows had less crimp (average  $\sim 0.15\%$ ); the failure strain measured was between 1.35 and 1.85%. Further investigation will be necessary to establish the axial fibre tow crimp's contribution to the triaxially braided composite failure strain.

The hoop layers introduced by the filament winding in the braid-winding hybrid lay-up experienced extensive splitting. This affects damage evolution and ultimate load carrying capability of the structure. Improvement in damage propagation was observed when the failure mechanisms of CP and OWB structures were compared in this study. Hence, further investigation on multiaxial layup developed using braid-winding will be necessary to explore structural damage development based on the findings of this study.

**Acknowledgements** The authors wish to thank Mr Edward William Godwin and Mr Christopher Cowan from National Composites Certification and Evaluation Facility (NCCCF) and the mechanical workshops of the school of materials in the University of Manchester for their support to carry out the research work.

**Open Access** This article is distributed under the terms of the Creative Commons Attribution 4.0 International License (<http://creativecommons.org/licenses/by/4.0/>), which permits unrestricted use, distribution, and reproduction in any medium, provided you give appropriate credit to the original author(s) and the source, provide a link to the Creative Commons license, and indicate if changes were made.

## References

1. Potluri, P.: Braiding. In: Nicolais, L., Borzacchiello, A., Lee, S.M. (eds.) *International Encyclopedia of Composites* vol. 1. Wiley, New York (2012)
2. Kyosev, Y.: *Braiding Technology for Textiles*. Elsevier Science, Amsterdam (2014)
3. Phoenix, S.: Mechanical response of a tubular braided cable with an elastic core. *Text. Res. J.* **48**, 81–91 (1978)
4. Swanson, S.R., Smith, L.V.: Comparison of the biaxial strength properties of braided and laminated carbon fiber composites. *Compos. Part B* **27**, 71–77 (1996)

5. Falzon, P.J., Herszberg, I.: Mechanical performance of 2-D braided carbon/epoxy composites. *Compos. Sci. Technol.* **58**, 253–265 (1998)
6. Harte, A.-M., Fleck, N.A.: On the mechanics of braided composites in tension. *Eur. J. Mech. A Solids* **19**, 259–275 (2000)
7. Smith, L.V., Swanson, S.R.: Micro-mechanics parameters controlling the strength of braided composites. *Compos. Sci. Technol.* **54**, 177–184 (1995)
8. Ivanov, D.S., Baudry, F., Van Den Broucke, B., Lomov, S.V., Xie, H., Verpoest, I.: Failure analysis of triaxial braided composite. *Compos. Sci. Technol.* **69**, 1372–1380 (2009)
9. Kohlman, L.W., Bail, J.L., Roberts, G.D., Salem, J.A., Martin, R.E., Binienda, W.K.: A notched coupon approach for tensile testing of braided composites. *Compos. A: Appl. Sci. Manuf.* **43**, 1680–1688 (2012)
10. Masters, J.E., Ifju, P.G.: A phenomenological study of triaxially braided textile composites loaded in tension. *Compos. Sci. Technol.* **56**, 347–358 (1996)
11. Byun, J.-H.: The analytical characterization of 2-D braided textile composites. *Compos. Sci. Technol.* **60**, 705–716 (2000)
12. West, A.C., Adams, D.O.: Axial yarn crimping effects in braided composite materials. *J. Compos. Mater.* **33**, 402–419 (1999)
13. Rawal, A., Saraswat, H., Sibal, A.: Tensile response of braided structures: a review. *Text. Res. J.* **85**, 2083–2096 (2015)
14. Roy, S.S., Zou, W., Potluri, P.: Influence of braid carrier tension on carbon fibre braided preforms. In: Kyosev, Y. (Ed.) *Recent Developments in Braiding and Narrow Weaving*, pp. 91–102. Cham: Springer International Publishing (2016)
15. Potluri, P., Manan, A., Francke, M., Day, R.J.: Flexural and torsional behaviour of biaxial and triaxial braided composite structures. *Compos. Struct.* **75**, 377–386 (2006)
16. A. D3171-15, Standard Test Methods for Constituent Content of Composite Materials, ASTM International, West Conshohocken, PA, [www.astm.org](http://www.astm.org) (2004)
17. A. D. D5450M-93, ASTM D5450 / D5450M-16, Standard Test Method for Transverse Tensile Properties of Hoop Wound Polymer Matrix Composite Cylinders. ASTM International, West Conshohocken, PA, ed, A. (2012)
18. Littell, J.D., Binienda, W.K., Roberts, G.D., Goldberg, R.K.: Characterization of damage in triaxial braided composites under tensile loading. *J. Aerosp. Eng.* **22**, 270–279 (2009)
19. Potluri, P., Thammandra, V.S.: Influence of uniaxial and biaxial tension on meso-scale geometry and strain fields in a woven composite. *Compos. Struct.* **77**, 405–418 (2007)